Synergistic interaction between the γ-Al_2O_3 washcoat and Cu-SSZ-13 for enhancing NH_3-SCR performance

Ruibin Sun[a], Yu Lyu[a,b], Chonglin Song[a,*], Chenxi Wang[a,c], Gang Lyu[a], Xiangyu Dong[a], Lei Tian[a], Xinhui Liu[a], Yibo Xu[a]

[a] State Key Laboratory of Engines, Tianjin University, Tianjin 300072, China

[b] China Automotive Engineering Research Institute Co., Ltd, Chongqing 401122, China

[c] Institute for Transport Studies, University of Leeds, Leeds LS2 9JT, UK

*Corresponding author： Chonglin Song

Postal address: State Key Laboratory of Engines, Tianjin University, Tianjin 300072, China

E-mail: songchonglin@tju.edu.cn

Abstract

The development of coated monolithic catalysts that combine high catalytic activity with high N_2 selectivity remains a significant challenge for NOx abatement in diesel exhaust gas. The slurry with Cu-SSZ-13 (CS), silica sol and γ-Al_2O_3 derived from alumina sol calcination was deposited on honeycomb cordierite monolith (CC) to obtain coated monolithic catalysts. This study aims to unravel the synergistic interaction between the γ-Al_2O_3 washcoat and CS as an active component to enhance the catalytic performance of CS. The CS-SiAl-4/CC displays excellent NOx purification performance in the absence of water vapor as well as outstanding hydrothermal aging resistance. The results indicate that γ-Al_2O_3 exhibits excellent adhesion and uniform dispersion on the CS surface without disrupting CS's crystalline structure. The coordination environment, redox properties and amount of Cu species are not affected by γ-Al_2O_3. Furthermore, γ-Al_2O_3 features a substantial number of both Brønsted and Lewis acid sites, which play a crucial role in storing NH_3 and providing NH_4^+. In situ DRIFTS results demonstrate that CS-SiAl-4/CC can adsorb more NOx species (free ionic nitrates and monodentate nitrates), which react with NH_3 adsorbed on the Lewis acid sites through the Langmuir-Hinshelwood (L-H) mechanism. NH_4^+ plays a more important role as the main active intermediates, and its reaction with gaseous NO suggests the Eley-Rideal (E-R) mechanism. More importantly, bidentate nitrates can

convert to monodentate nitrites, which serve as the active species for the SCR reaction. This phenomenon is likely the main reason for the superior SCR performance of CS-SiAl-4/CC compared to CS-Si/CC.

Keywords: Synergistic interaction, γ-Al_2O_3, Cu-SSZ-13, NH_3-SCR, Coated monolithic catalysts

1. Introduction

Nitrogen oxides (NOx) derived from automobiles, construction machinery, ships, agriculture, electric power and other fields have been recognized as one of pollutants in the atmosphere and have severely threatened the global ecological environment and human health [1–5]. Therefore, controlling NOx emissions will continue to be a high profile issue in many countries in forthcoming periods. Currently, selectivity catalytic reduction of NOx by ammonia (NH_3-SCR) has been proven to be one of the most widely utilized and most effective exhaust gas purification methods for NOx elimination in the today's world [6,7]. State-of-the-art commercial Cu-SSZ-13 catalysts, as the core component of the catalytic reaction in the monolithic catalysts, have played a key role in the NH_3-SCR technology. However, it has been confronted with some very tricky technical challenges (e.g. hot airflow at high space velocity and complex exhaust atmospheres) in maintaining high catalytic performance in industrial applications. Therefore, the development of coated monolithic catalysts with high catalytic activity and N_2 selectivity has become an urgent problem to be solved.

Currently, monolithic catalysts consist of support, washcoat (also known as a secondary support) and active component. Honeycomb cordierite monolith ($2MgO{\cdot}2Al_2O_3{\cdot}5SiO_2$), as a significant inorganic non-metallic porous structure material, is generally considered to be the best denitration catalyst support due to its advantages of low heat capacity and thermal expansion coefficient, thermal shock resistance and low pressure drop [8,9]. Nevertheless, to facilitate the adequate loading, dispersion, and stabilization of the active components on its surface, it is often necessary to apply pre-deposited support components and carry out pre-treatment on the surface of the honeycomb cordierite monolith with a very small specific surface area before loading the active component [10–14]. Although the prepared coated monolithic catalysts have met the anticipated loading capacity and catalytic performance, there are certain drawbacks associated with this preparation method, including numerous impregnation cycles, a cumbersome preparation process and a relatively low loading capacity per cycle. In addition, the monolithic catalysts prepared by the coating method involve

formulating a catalyst slurry with a specific proportion of catalyst precursors, water, binders, surfactants, etc., and then the slurry is deposited on the surface of honeycomb cordierite monolith to form a monolithic catalyst with a catalyst precursor coating. Compared with the pretreatment and pre-deposition of the support, this method for obtaining monolithic catalysts is simpler, requires less raw material and achieves a higher catalyst utilization rate, and monolithic catalysts prepared by the coating method have been applied in some fields. For instance, Xu et al. [15], Tang et al. [16] and Lisi et al. [17] discovered that the catalysts obtained by the coating method exhibited excellent catalytic performance in terms of NOx reduction, NO catalytic oxidation and NO decomposition, respectively.

Currently, binders are divided into organic binder (e.g., methyl 2-hydroxyethyl cellulose, polyvinyl alcohol and polyethylene glycol) and inorganic binder (e.g., colloidal silica, alumina sol and titania sol) according to their chemical composition. However, the binders, as one of the most critical raw materials for coated monolithic catalyst, could directly affect the catalytic performance, selectivity and stability of the coated monolithic catalyst to a certain extent. Shi et al. [18] pointed out that boehmite and zirconium oxynitrate as suitable binders could be effective in forming the Fe clusters with an excellent NO oxidation and storage abilities in the reaction temperature range of 100–300 ℃ and Fe^{3+} with an outstanding NO oxidation performance in the reaction temperature range of 400–650 ℃, respectively, thereby resulting in the coated Fe based catalysts with distinct catalytic activities. Zhang et al. [19] reported that Al_2O_3 derived from alumina gel precursor could improve the redox properties of Fe species more than SiO_2 originated from silica gel precursor for Fe/BEA catalysts, but Fe/BEA catalyst doped with Al_2O_3 or SiO_2 exhibited very similar pore structures. Therefore, the selected binders are particularly critical in terms of automobile exhaust denitrification. Nowadays, catalysts supported on Al_2O_3, CeO_2, TiO_2 and SnO_2 have attracted the attention of researchers [20–23]. For instance, γ-Al_2O_3, also known as activated alumina, is widely used as a catalyst support due to its large specific surface area, abundant pore structure, excellent adsorption properties, and favorable surface acidity. Yao et al. [24] compared SiO_2, γ-Al_2O_3, ZrO_2 and TiO_2 as four commonly used catalyst supports in industry, and reported that γ-Al_2O_3 can improve the catalytic performance of Ce-based catalysts through the fast NH_3-SCR pathway. Zhou et al. [25] indicated that Al_2O_3 could provide abundant Lewis acid sites, which could accelerate the formation of intermediate products (NO_2 or NO_3^-), thus enhancing the catalytic performance over a broad temperature range (>350 ℃) and the N_2 selectivity within a higher temperature range (>450 ℃). Therefore, the above research results can

provide a strong theoretical basis for the selection of binders that are satisfied with industrial applications. Additionally, the selected binders can not only be effective in enhancing the adhesion between the active component and the cordierite surface and the single-time loading capacity of active components during the preparation of the coated catalysts, but also the product produced by the binders during the calcination process can form a synergistic effect with the active component to improve the catalytic activity of the catalyst in the NH_3-SCR catalytic reactions. However, there is comparatively little research focusing on the interaction between the washcoat generated by the inorganic binder during the calcination process and Cu-SSZ-13 as the active component for the coated monolithic catalysts.

In the present work, a series of coated monolithic catalysts were prepared onto honeycomb cordierite monoliths (CC) by using the slurry coating method. This study aims to unravel the synergistic interaction between the γ-Al_2O_3 washcoat (produced by calcination of alumina sol) and Cu-SSZ-13 as an active component for achieving efficient NOx removal. In addition, the synergistic interaction is further revealed through a comprehensive investigation of the structure and textural properties, redox properties, electrostatic interactions, NOx/NH_3 adsorption-desorption behavior and catalytic reaction mechanism.

2. Experiment and Method

2.1 Preparation of coated monolithic catalysts

The catalyst slurry was prepared by physically mixing the commercial Cu-SSZ-13 (CS) with a SiO_2/Al_2O_3 molar ratio of 20 and Cu content of 4.12 wt%, the deionized water, the binder (silica sol with a 30 wt% SiO_2 and alumina sol with a 10 wt% AlOOH) and the dispersing agent in a mass ratio of 32:64:20:1. The solid content and pH value of the catalyst slurry were maintained at 32.5 wt% and 4.65, respectively. The mass ratio of silica sol and alumina sol was 6:1, 5:1, 4:1 and 3:1, respectively. Subsequently, the slurry was stirred on a magnetic stirrer for 48 h under 500 rpm to form a mixed stable catalyst slurry.

The catalyst slurry was deposited in honeycomb cordierite monolith (CC) with a square channel density of 300 cpsi (cells per square inch), a length of 30 mm, a diameter of 20 mm and a wall thickness of 0.18 mm. The excess slurry retained in the straight channel was blown off by compressed air to avoid clogging the channels. The coated monolithic catalyst was dried in an electrothermal blast drying

oven at 110 ℃ (at a heating rate of 2 ℃·min^{-1}) for 24 h and calcined in a muffle oven at 550 ℃ (at a heating rate of 5 ℃·min^{-1}) for 4 h. This coating process was repeated several times until the desired coating loading of 36 wt% was deposited onto the CC. The prepared catalysts were designated as Al/CC, CS-Si/CC and CS-SiAl-*x*/CC, where CS, Si, Al and *x* stand for CS, SiO_2, γ-Al_2O_3 and the ratio of SiO_2 to γ-Al_2O_3 mass of 6, 5, 4 and 3, respectively. In addition, the Cu content was measured by ICP-OES and listed in Table 1. The Cu content in the catalysts is approximately 3.40 wt%.

Table 1 Physicochemical properties of CS, CS-Si/CC and CS-SiAl-*x*/CC.

catalysts	[a] Cu content (wt%)	[b] Relative crystallinity (%)	[c] Specific surface area ($m^2 \cdot g^{-1}$)	[d] Micropore volume ($m^3 \cdot g^{-1}$)
CS	4.12	100	582.20	0.21
CS-Si/CC	3.46	98.29	530.67	0.18
CS-SiAl-6/CC	3.46	97.58	528.28	0.17
CS-SiAl-5/CC	3.47	97.19	530.85	0.18
CS-SiAl-4/CC	3.45	98.81	531.33	0.17
CS-SiAl-3/CC	3.21	97.89	479.24	0.14

[a] Analyzed by ICP-OES. [b] Analyzed by XRD [c] Analyzed by BET method. [d] Analyzed by t-plot method.

(Relative crystallinity $= \frac{\text{peak area of } (2\theta = 9.5° + 12.9° + 14.1° + 16.0° + 17.8° + 20.6° + 25.1° + 30.6°)_m}{\text{peak area of } (2\theta = 9.5° + 12.9° + 14.1° + 16.0° + 17.8° + 20.6° + 25.1° + 30.6°)_n} \times 100\%$, where m and n represented CS-Si/CC(CS-SiAl-*x*/CC) and CS, respectively).

2.2. Characterization of coated monolithic catalyst

The elemental contents of Si, Al and Cu in the catalyst were studied by inductively coupled plasma-optical emission spectrometry (ICP-OES).

The structural properties of the catalysts were carried out on a Rigaku D/MAX-2500 instrument manufactured by Rigaku Corporation, utilizing Cu-Kα as a radiation source (λ = 0.154 nm) and employing the tube voltage at 40 kV and current at 40 mA. Real-time data was recorded for 2θ values from 10 to 90° with a step size of 0.02 and a scanning speed of 5°·min^{-1}.

The microstructure characteristics and element distribution of the catalysts were observed by means of scanning electron microscope (SEM) and energy dispersive spectrometer (EDS).

The textural properties of the catalysts were determined by an ASAP 2020C instrument. The catalysts were pretreated under vacuum at 350 ℃ for 9 h, and then the treated catalyst was tested in a liquid nitrogen environment. The adsorption-desorption isotherms were measured at -196 ℃ and in a helium (He) atmosphere. The specific surface area and micropore volume were computed.

The elemental composition and chemical valence on the surface of the catalysts were analyzed on an Axis Supra spectrometer, utilizing a monochromatic Al-Kα X-ray source and using the C1s orbital at a binding energy of 284.8 eV to carry out the charge correction. The coordination environment of Cu species of the catalysts was verified by using UV–vis diffuse reflectance spectroscopy (UV–vis DRs).

Temperature-programmed reduction tests including H_2-temperature-programmed reduction (H_2-TPR) and NH_3/NO-temperature-programmed desorption (NH_3/(NO + O_2)-TPD) were researched on a ChemBET Pulsar TPR/TPD automatic temperature-programmed chemical analyzer. All catalysts were processed at 400 ℃ in an Ar atmosphere with 50 mL·min^{-1} for 2 h to eliminate the adsorbed impurities from the catalyst surface and subsequently cooled to 50 ℃. For the H_2-TPR test, 50 mg catalyst with 40-60 mesh was heated from 50 to 800 ℃ at a heating rate of 5 ℃·min^{-1} in 1% H_2/Ar with 110 mL·min^{-1}. Before NH_3/NO-TPD test, it was saturation adsorption in 10% NH_3/Ar or 10% NO/Ar + 10 vol% O_2 with 110 mL·min^{-1} at 50 ℃ for 2 h. Subsequently, it was heated again from 50 to 800 ℃ at a heating rate of 5 ℃·min^{-1} under a pure Ar with 110 mL·min^{-1}.

The evolution of NOx and/or NH_3 adsorption and desorption species and intermediate species on the catalysts was investigated by in-situ diffuse reflectance infrared fourier transform spectroscopy (In situ DRIFTS) online analysis, coupled with a liquid-nitrogen-cooled mercury cadmium telluride (MCT) detector. The catalyst sample is diluted with KBr at a dilution ratio of 1:100. Prior to testing, a pure Ar gas with 100 mL·min^{-1} was passed from the sample at 400 ℃ for 2 h in order to clean trace impurities from the samples and subsequently cooled to the desired reaction temperature. In the process of testing, the feed reactant gas (1100 ppm NH_3 (when used), 1000 ppm NO (when used) and 10 vol% O_2 (when used)) was passed through the samples, and the total flow of the feeding gas was 50 mL·min^{-1}.

2.3. Coated monolithic catalyst activity evaluation

The coated monolithic catalyst activity evaluation was carried out in a fixed-bed reactor made of a quartz tube at atmospheric pressure. The target reaction temperature in the reactor and reaction gas flow rate were precisely controlled by a series of K-type thermocouples as well as PID control furnaces and the mass flow controllers. The coated monolithic catalyst was placed into the reactor with an inner diameter of 20 mm. The catalytic reaction of NOx by NH_3 was performed in the temperature range of 150–550 ℃ (interval 50 ℃), and the feed gas contained 1100 ppm NH_3, 1000 ppm NO and 10 vol% O_2 with Ar as the balance gas and maintained the gas hourly space velocity (GHSV) at 70,000 h^{-1} (total

flow rate of 8.110 L·min^{-1}). To investigate the effect of hydrothermal aging on the activity of monolithic catalyst, the monolithic catalyst was pretreated at 800 ℃ for 12 h in 10 vol% water vapor (only used for the hydrothermal aging research). During the experiment, the steady-state outlet concentrations (NO, NH_3, N_2O and NO_2) were measured by an online mass spectrometer manufactured by V&F corporation from Austria. The key parameters for evaluating the catalytic performance of monolithic catalysts were treated as equations (1) and (2) :

$$\text{NOx conversion} = \frac{C_{\text{NO,in}} - C_{\text{NO,out}}}{C_{\text{NO,in}}} \times 100\% \quad (1)$$

$$\text{N}_2 \text{ selectivity} = 1 - \frac{2C_{\text{N}_2\text{O,out}} + C_{\text{NO}_2\text{,out}}}{C_{\text{NO,in}} - C_{\text{NO,out}} + C_{\text{NH}_3\text{,in}} - C_{\text{NH}_3\text{,out}}} \times 100\% \quad (2)$$

where $C_{g,in}$ and $C_{g,out}$ denote feed and effluent gases concentration of species g.

3. Results and Discussion

3.1 NH_3-SCR catalytic performance

Fig. 1 depicts the changes in NOx conversion and N_2 selectivity of Al/CC and CS-Si/CC and CS-SiAl-*x*/CC (*x* = 3, 4, 5 and 6) in the temperature range of 150 to 550 ℃. The Al/CC displays virtually no activity for the NH_3-SCR reaction over the tested temperature range of 150 to 550 ℃, with the NO conversion remaining around 7% (Fig 1(a)). In addition, the variation trends in NOx conversion and N_2 selectivity for CS-Si/CC and CS-SiAl-*x*/CC exhibit a remarkable similarity at different temperatures. It can be clearly observed from Fig. 1(a) that the CS-Si/CC achieves a NOx conversion exceeding 80% within the temperature region of 260–500 ℃, with the maximum NOx conversion of 86.83% occurring at 300 ℃. Furthermore, CS-SiAl-*x*/CC displays an exceptionally high NOx conversion than CS-Si/CC in the whole temperature window. In addition, there are significant differences in catalytic performance between CS-SiAl-4/CC and CS-SiAl-3/CC. This suggests that the introduction of excessive γ-Al_2O_3 may cover the active sites or block the pores of CS, thereby leading to a decline in catalytic performance. However, the enhancement effects of CS-SiAl-4/CC are particularly pronounced. The CS-SiAl-4/CC maintains the NOx conversion in excess of 80% at 218–550 ℃ and 90% at 245–440 ℃, reaching a maximum NOx conversion of 96.27% at 300 ℃. These results indicate that γ-Al_2O_3 effectively broadens the reaction temperature window for achieving over 80% NOx conversion and significantly enhances catalytic activity in the entire temperature range. In

addition, a noticeable decreasing trend in the NOx conversion is detected for all catalysts when the reaction temperature surpasses 400 ℃, this phenomenon can be explained by the non-selective oxidation of reducing agent NH_3 with O_2 [26]. As depicted in Fig. 1(b), compared with CS-Si/CC, CS-SiAl-*x*/CC demonstrates remarkably superior N_2 selectivity and maintains the N_2 selectivity of above 98% at 200–550 ℃ in the NH_3-SCR reaction. For all catalysts, NO_2 by-product is discovered at below 250 ℃, whereas the formation of N_2O as a byproduct takes place at above 250 ℃ (Fig. S1). Furthermore, the N_2 selectivity of the CS-SiAl-*x*/CC gradually increases with the rise of γ-Al_2O_3 content, which indicates that γ-Al_2O_3 can effectually improve the N_2 selectivity of the catalyst.

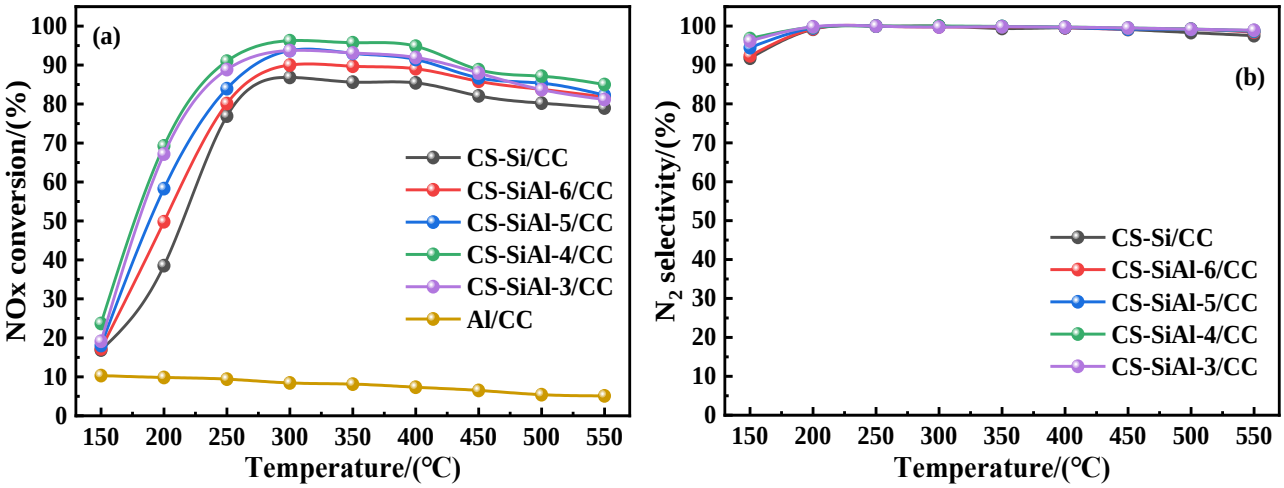

Fig. 1. (a) NOx conversion and (b) N_2 selectivity of Al/CC, CS-Si/CC and CS-SiAl-*x*/CC.

It is well-known that the hydrothermal aging treatment may affect the NH_3-SCR reaction in the diesel engine exhaust [26–29]. Therefore, the influence of hydrothermal aging on the performance of the catalyst was investigated. As shown in Fig. 2, there is a decline in the performance of the CS-Si/CC and CS-SiAl-*x*/CC within the temperature region of 150 to 550 ℃. CS-Si/CC exhibits a temperature window for NOx conversion above 80% between 286–431 ℃, but it does not achieve a NOx conversion above 85% at any temperature. In contrast, CS-SiAl-4/CC displays superior catalytic performance, achieving a temperature window for NOx conversion above 80% between 250–522 ℃ and above 90% between 289–415 ℃.

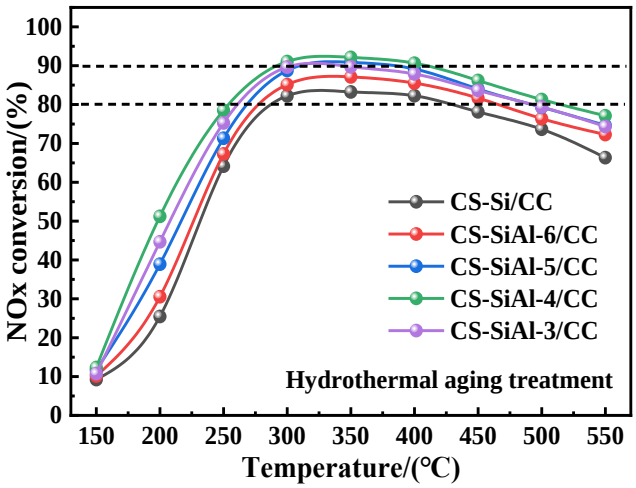

Fig. 2. NOx conversion of CS-Si/CC and CS-SiAl-*x*/CC after hydrothermal aging treatment.

3.2 Textural properties

The zeolite lattice structures of the CS and CS-SiAl-*x*/CC were detected by XRD technique. As depicted in Fig. 3, the major characteristic diffraction peaks of CS-Si/CC and CS-SiAl-*x*/CC at 2θ angles of 9.5°, 12.9°, 14.1°, 16.0°, 17.8°, 20.6°, 25.1° and 30.6° are in accordance with standard SSZ-13 (PDF# 47–0762). In addition, compared to the CS, no significant changes are observed in the major characteristic diffraction peaks and signal intensity after the introduction of γ-Al_2O_3 derived from alumina sol calcination or SiO_2 formed via silica sol calcination, which reveals that the framework structure of CS is not destroyed by the introduction of silica sol and alumina sol during the preparation of the catalyst preparation. As can be seen from Fig. S2, the characteristic diffraction peak of SiO_2 at 2θ angle of 21.6° is consistent with the corresponding peak of standard SiO_2 (PDF# 27–0605), while the characteristic diffraction peaks of γ-Al_2O_3 at 2θ angles of 19.4°, 32.3°, 37.1°, 39.5°, 45.9°, 60.8° and 66.9° correspond to those of standard γ-Al_2O_3 (PDF# 10–0425). The major characteristic diffraction peaks attributable to γ-Al_2O_3 and SiO_2 are exhibited during calcination when pure silica sol and pure alumina sol are mixed, demonstrating that the γ-Al_2O_3 or SiO_2 species are not affected by the preparation conditions. Furthermore, all catalysts do not display a diffraction peak attributable to SiO_2 or γ-Al_2O_3 or CuO, which illustrates that the SiO_2 or γ-Al_2O_3 is uniformly dispersed on the surface of CS, and there is no release of Cu species when the silica sol and alumina sol are introduced during the preparation of the catalyst. Moreover, the relative crystallinity of the catalyst was calculated by the peak areas at 2θ = 9.5°, 12.9°, 14.1°, 16.0°, 17.8°, 20.6°, 25.1° and 30.6° [30]. As shown in Table 1, CS-Si/CC and CS-SiAl-*x*/CC exhibit a similar relative crystallinity (97–98%), which is slightly lower

than that of CS (100%). This result indicates that SiO_2 and γ-Al_2O_3 do not affect the framework structure of SSZ-13. In addition, the study finds no significant correlation between the relative crystallinity and catalytic activity in the SCR reaction.

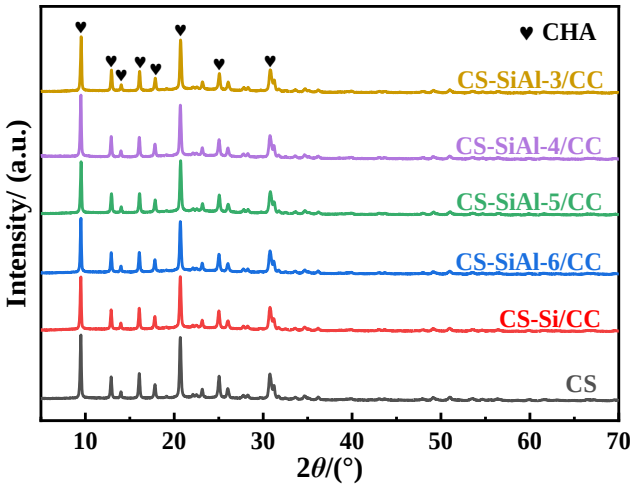

Fig. 3. XRD patterns of CS, CS-Si/CC and CS-SiAl-*x*/CC.

The microstructure and element distribution of the CS, CS-Si/CC and CS-SiAl-*x*/CC (*x* = 3 and 4) were investigated by SEM and EDS in Fig. 4 and Fig. S3. It is observed from the SEM of Fig. 4 that CS consists of particles exhibiting nearly cubic morphology with sizes of 0.25–0.30 μm. The introduction of SiO_2 and γ-Al_2O_3 does not change the approximately cubic morphology of CS-Si/CC and CS-SiAl-4/CC, demonstrating that the SiO_2 and γ-Al_2O_3 do not destroy the structural integrity of the CS framework. In addition, small particles are observed on the cubic surfaces of CS-Si/CC and CS-SiAl-4/CC. Small particles exhibit excellent adhesion and uniform dispersion on the cubic surfaces of the CS, as evidenced by SEM imaging (Fig. 4). To confirm the elemental composition of CS-Si/CC and CS-SiAl-4/CC, the EDX measurement was carried out. As depicted in Fig. S3, the elements of CS-Si/CC and CS-SiAl-4/CC are composed of O, Si, Al and Cu. Elemental mapping clearly demonstrates that O, Si, Al and Cu are uniformly distributed in the CS-Si/CC and CS-SiAl-4/CC. Furthermore, the Cu contents in CS-Si/CC and CS-SiAl-4/CC measured by EDX are 3.77 and 3.71 wt% (Fig. S3), respectively, which suggests that the elements are uniformly distributed. However, agglomeration is observed in the CS-SiAl-3/CC (Fig. 4). According to the characterization by XRD, the signal intensity of the characteristic peaks in CS-SiAl-3/CC is essentially comparable to that in CS. These findings indicate that excessive γ-Al_2O_3 can lead to the agglomeration of CS.

The structure of the catalysts was examined by He-physisorption. The results in Table 1 display

that CS-Si/CC features a micropore volume of 0.18 $m^3 \cdot g^{-1}$ and a specific surface area of 530.67 $m^2 \cdot g^{-1}$. After the introduction of γ-Al_2O_3, CS-SiAl-*x*/CC (*x* = 4, 5 and 6) exhibits no change in micropore volume and specific surface area compared to CS-Si/CC. However, compared to CS-SiAl-4/CC, CS-SiAl-3/CC possesses a micropore volume of 0.14 $m^3 \cdot g^{-1}$ and a specific surface area of 479.24 $m^2 \cdot g^{-1}$, reducing by 9.80% and 17.65%, respectively. Combined with SEM characterization results, the deterioration in the structure of CS-SiAl-3/CC is attributed to the agglomeration of CS, which consequently decreases its performance.

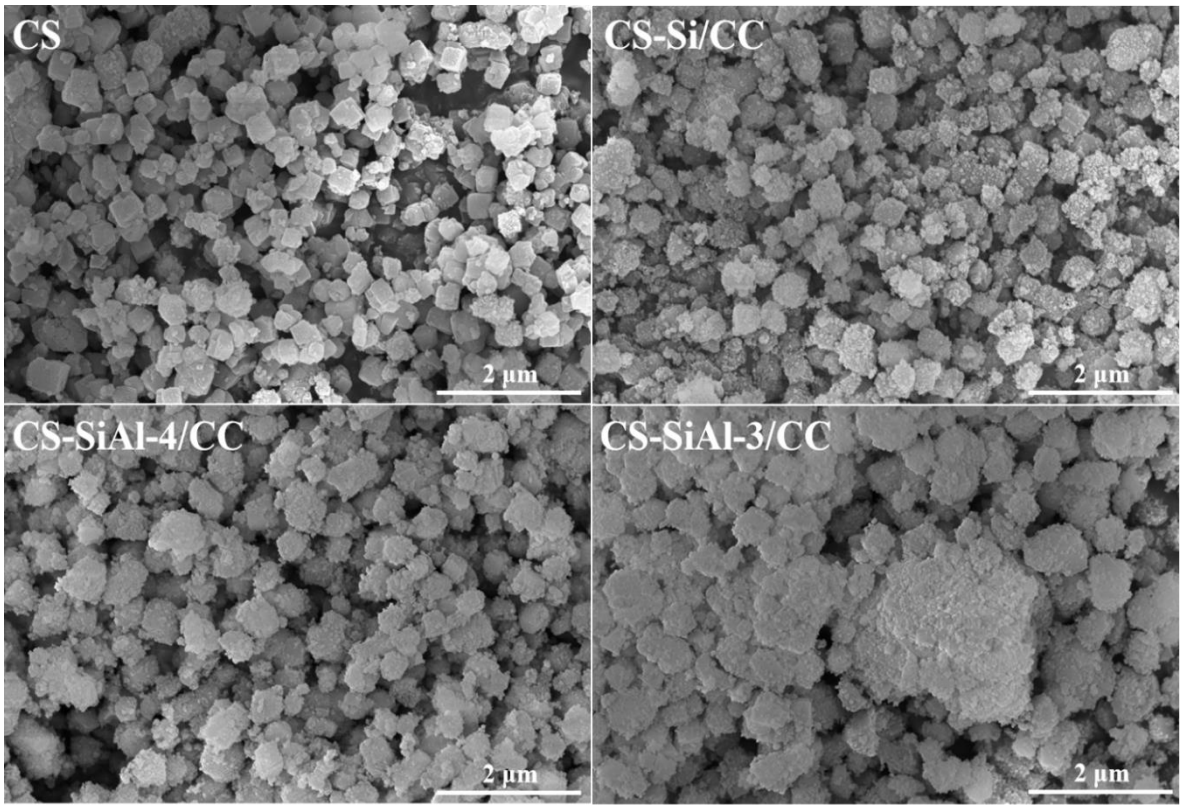

Fig. 4. SEM images of CS, CS-Si/CC, CS-SiAl-4/CC and CS-SiAl-3/CC.

3.3 Active Cu species

The Cu^{2+} is always recognized by researchers as the active center of the adsorption and oxidation of NH_3 or NO in the NH_3-SCR reaction, involving $[ZCu^{2+}(OH)]^+$ located at eight-member rings (8MRs) and Z_2Cu^{2+} located at six-member rings (6MRs) (Z stands for a molecular sieve framework negative charge) [31,32]. Therefore, the redox properties of the Cu^{2+} in the CS-Si/CC, CS-SiAl-*x*/CC and CS were characterized by H_2-TPR, and the results are depicted in Fig. 5(a) and Fig. S4(a). For CS-Si/CC, CS-SiAl-*x*/CC and CS, four deconvoluted peaks of H_2 consumption from 100–500 ℃ can be found at around 220, 297, 380 and 445 ℃, which are designated as the reduction of $[ZCu^{2+}(OH)]^+$ located at

the 8MRs to Cu^{+} [15,28], the reduction of CuO to Cu^{0} [28,33], the reduction of Z_2Cu^{2+} located at the 6MRs to Cu^{+} [33,34] and the reduction of Cu^{+} to Cu^{0} [35,36], respectively. CS-Si/CC and CS-SiAl-*x*/CC (*x* = 4, 5 and 6) are almost identical in terms of H_2 consumption amount on $[ZCu^{2+}(OH)]^{+}$ sites (at approximately 85.21 μmol·g^{-1}), Z_2Cu^{2+} sites (at approximately 192.03 μmol·g^{-1}) and total H_2 consumption amount (at approximately 277.24 μmol·g^{-1}) in Table 2 and H_2 reduction temperature (at around 220, 297, 380 and 445 ℃, respectively) in Fig. 5(a) and Fig. S4(a), which declares that the redox properties of Cu^{2+} are not affected by the presence of SiO_2 and γ-Al_2O_3. This finding exhibits an inverse trend compared to catalysts synthesized through mechanical blending [15] or ion-exchange methods [30], indicating that the differences in catalyst preparation methods directly influence the H_2 reduction temperature and H_2 consumption amount of Cu active sites. However, the presence of excess γ-Al_2O_3 leads to partial coverage of Cu active sites in CS, thereby inducing the decrease of H_2 consumption amount. In addition, excessive γ-Al_2O_3 does not affect the reduction temperature of Cu species.

The element chemical states and chemical composition of the catalysts were characterized by XPS analysis and the surface atomic concentrations of the catalyst were summarized in Table S1. The results indicate that Si, Al and O are the main elements on the catalyst surface, whereas the content of Cu element is very low. Furthermore, the Cu contents in CS-Si/CC and CS-SiAl-*x*/CC (*x* = 4, 5 and 6) are similar, indicating that the difference in catalyst performance is attributed to γ-Al_2O_3. In contrast, the Cu contents in CS-SiAl-3/CC are lower than those in other catalysts.

The XPS was further carried out to confirm the effect of SiO_2 and γ-Al_2O_3 on Cu species in the catalysts. The Cu 2p XPS spectra of CS-Si/CC, CS-SiAl-*x*/CC in Fig. 5(b) and CS in Fig. S4(b) were displayed. Cu $2p_{3/2}$ and Cu $2p_{1/2}$ peaks can be detected in the range of 930.3-938.9 and 950.4-956.3 eV, respectively [37–39]. Additionally, there is a peak at around 944.3 eV, which is attributed to the shake-up satellites [40,41], illustrating that the valence state of the Cu species in the CS-Si/CC and CS-SiAl-*x*/CC is predominantly + 2. The Cu $2p_{3/2}$ peaks can be divided into two contributions appearing at around 936.4 and 933.5 eV, which are designated as Cu^{2+} associated with oxygen atom sites in the framework structure of the molecular sieve (Cu-O-Si-O) and CuO species, respectively [29,35,42,43]. It can be clearly found from Table 2 that the Cu^{2+} surface concentration on CS-Si/CC and CS-SiAl-*x*/CC (*x* = 4, 5 and 6) remains nearly constant at approximately 0.16 at%, which suggests that there is no change in the Cu species with the introduction of SiO_2 and γ-Al_2O_3. Furthermore,

surface Cu^{2+} concentration on the CS-SiAl-3/CC decreases when excess γ-Al_2O_3 is introduced. This result is in line with the H_2-TPR.

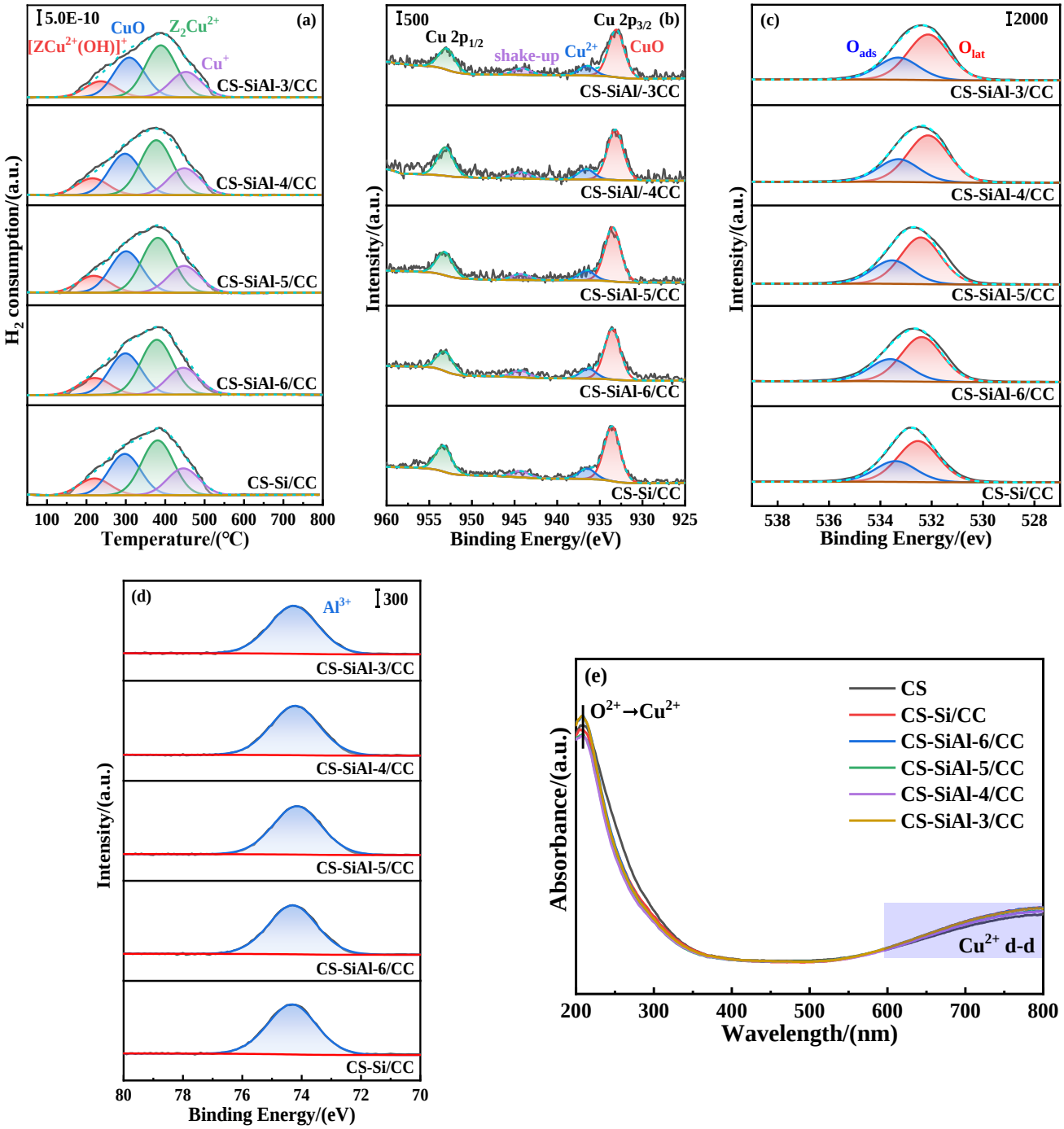

Fig. 5. (a) H_2-TPR, (b) Cu 2p XPS, (c) O 1s XPS, (d) Al 2p XPS and (e) UV–vis DRS spectra of CS-Si/CC and CS-SiAl-*x*/CC.

The catalysts' O 1s spectra illustrated in Fig. 5(c) and Fig. S4(c) can be divided into lattice oxygen (O_{lat}) at 532.1-532.6 eV and chemisorption oxygen (O_{ads}) at 533.2-534.6 eV [30,44]. In addition, the O_{ads} exhibits greater activity than O_{lat} due to its high mobility, thus facilitating the NH_3-SCR reaction

[45]. Therefore, the proportion of $O_{ads}/(O_{lat} + O_{ads})$ of the catalysts was calculated from the corresponding peak areas and listed in Table 2. The proportion of $O_{ads}/(O_{lat} + O_{ads})$ in the catalyst remains at approximately 33%, suggesting that the addition of SiO_2 and γ-Al_2O_3 cannot influence the O_{ads} of the catalysts. Hence, the difference in activity between CS-Si/CC and CS-SiAl-*x*/CC is not caused by O_{ads}. In Fig. 5d, a peak at around 74.3 eV corresponds to Al^{3+}, which indicates that Al exists primarily in the form of + 3 in the catalyst [46,47].

Table 2 Changes in concentration of Cu and O species on CS, CS-Si/CC and CS-SiAl-*x*/CC.

catalysts	[a] H_2 consumption (μmol·g^{-1})			[b] Surface Cu^{2+} concentration (at%)	[b] $O_{ads}/(O_{ads}+ O_{lat})$ (%)
	$[ZCu^{2+}(OH)]^+$	Z_2Cu^{2+}	Total		
CS	100.89	243.04	343.93	0.20	33.54
CS-Si/CC	85.24	192.07	277.31	0.16	33.59
CS-SiAl-6/CC	85.20	192.02	277.22	0.15	33.23
CS-SiAl-5/CC	85.39	192.63	278.02	0.15	33.43
CS-SiAl-4/CC	85.01	191.40	276.41	0.17	32.67
CS-SiAl-3/CC	80.12	173.79	252.91	0.12	32.70

[a] Analyzed by H_2-TPR. [b] Analyzed by XPS.

The UV–vis DRS spectra were used to further clarify the coordination environment of Cu species in the CS, CS-Si/CC and CS-SiAl-*x*/CC. As shown in Fig. 5e, an extremely significant absorption peak centered at around 205 nm and another weak and broad absorption peak in the range of 600-800 nm are observed for all the catalysts, which can be considered as the charge transferring by oxygen in molecular sieve framework structure to Cu^{2+} ($O^{2-}\rightarrow Cu^{2+}$) and the electron d-d transition of Cu^{2+} in dispersed CuO species with octahedral coordination, respectively [41,48–51]. Compared to CS, CS-Si/CC and CS-SiAl-*x*/CC exhibit almost no change in the strength and position of the adsorption peaks, indicating that the coordination environment of Cu species remains unaltered upon the introduction of SiO_2 and γ-Al_2O_3. This result is consistent with the XPS and H_2-TPR.

3.4 Adsorption/Desorption and activation of $NO+O_2$

3.4.1. $NO+O_2$ adsorption

As one of the major reactants, NOx on the catalyst is critical for adsorption, oxidation and desorption properties in the NH_3-SCR of NOx performance. The catalysts were pretreated in an Ar

atmosphere for 1 h at 400 ℃, followed by purging with Ar for 1 h at 50 ℃. Subsequently, a gas mixture of 1000 ppm NO + 10% O_2 was introduced and the adsorption of NO + O_2 on CS, CS-Si/CC and CS-SiAl-*x*/CC was recorded using in situ DRIFTS at 50 ℃. As exhibited in Fig. 6, the five distinct types of adsorbed NOx species are identified in all catalysts. The peaks at 1332 and 1423 cm^{-1} are assigned to monodentate nitrates adsorbed on Cu sites [35,52–54]. The peak at 1373 cm^{-1} is commonly derived from free ionic nitrates adsorbed on Cu sites [55,56], while those at 1589, 1628 and 1730 cm^{-1} are assigned to bidentate nitrates, bridging nitrates and absorbed N_2O_4, respectively [56–58]. Under the conditions of 50 ℃ and 10 min, the adsorbed NOx species on CS-Si/CC and CS-SiAl-*x*/CC remain unchanged compared with those on CS (Fig. 6a), indicating that the introduction of SiO_2 and/or γ-Al_2O_3 has no significant effect on the NOx adsorbed species on CS. The temporal evolution of adsorbed NOx species on CS, CS-Si/CC, and CS-SiAl-4/CC was investigated using in situ DRIFTS for real-time monitoring, as shown in Fig. 6b-d. The peak intensity of adsorbed NOx species exhibits a positive correlation with the exposure time to NO + O_2. Notably, the peak intensities corresponding to adsorbed NOx species on CS-SiAl-4/CC are markedly higher than those observed on CS and CS-Si/CC at the same time point. It can be inferred that the introduction of γ-Al_2O_3 drives a bifunctional mechanism that promotes NOx adsorption capacity and NOx adsorption rate. It is reported that monodentate nitrates, serving as key intermediates, can participate in the NH_3-SCR reaction [35,59,60], and thus more monodentate nitrates are formed over CS-SiAl-4/CC promoting the catalytic activity.

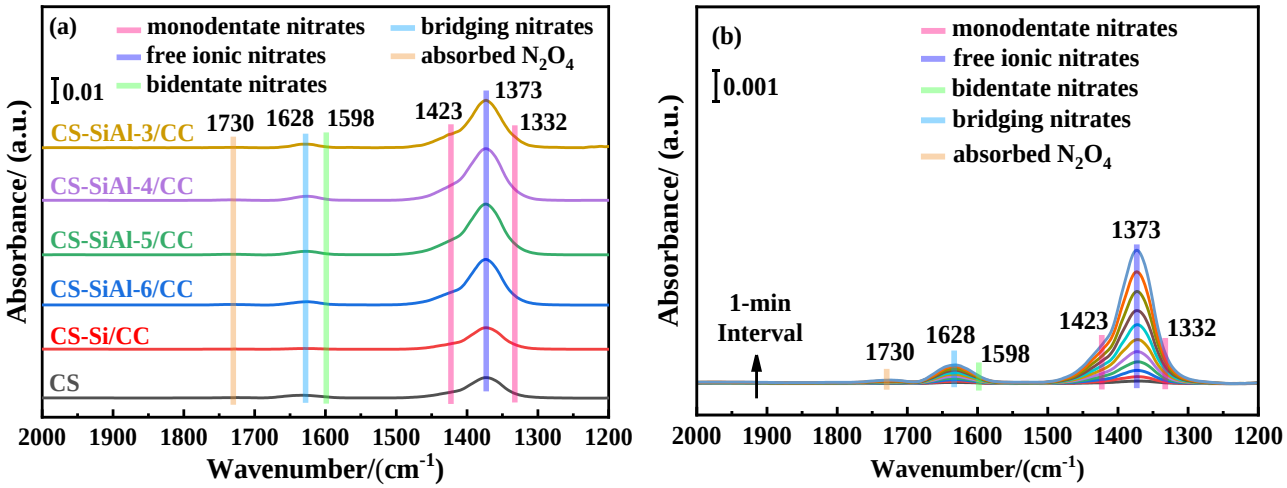

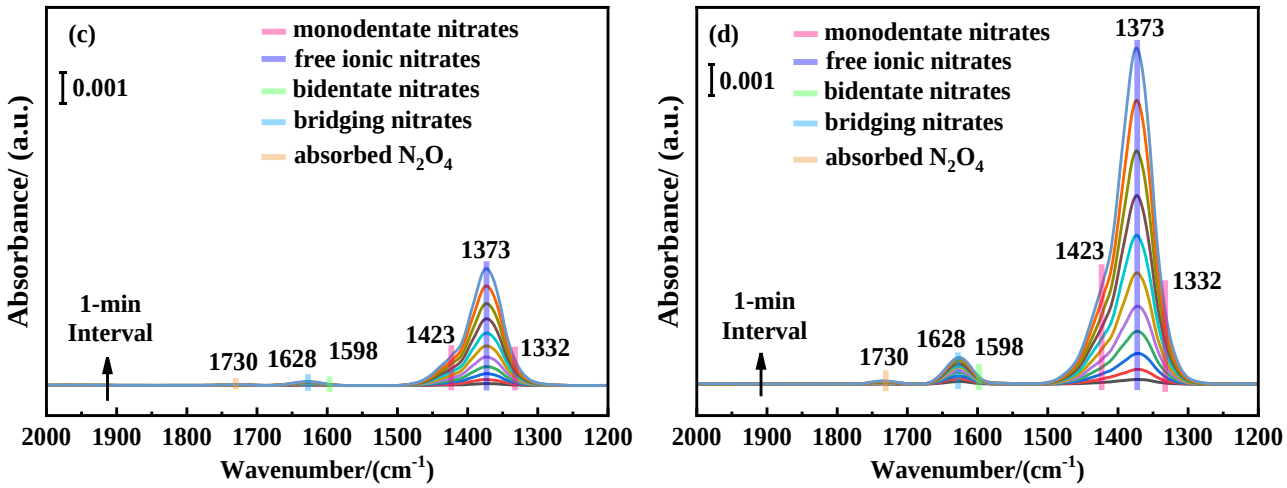

Fig. 6. In situ DRIFTS of $NO+O_2$ adsorption on: (a) CS, CS-Si/CC and CS-SiAl-*x*/CC at 50 ℃ at 10 min; (b)–(d) Time-dependent profiles for (b) CS, (c) CS-Si/CC and (d) CS-SiAl-4/CC with exposure durations spanning 1–10 min (at 1 min intervals) at 50 ℃.

3.4.2. $NO+O_2$ desorption

The desorption behavior of NOx at active sites of the catalyst was further investigated by $(NO+O_2)$-TPD, and the experimental results were displayed in Fig. 7 and Fig. S5. For the CS-Si/CC and CS-SiAl-*x*/CC, there are two peaks of NOx desorption in the temperature range of 50–200 and 225–445 ℃. It is interesting to note that γ-Al_2O_3 can be an effective NOx adsorbent. In contrast, SiO_2 has almost no effect on NOx adsorption (Fig. S5b). It can be observed from Table 3 that the amount of NOx desorption on CS-SiAl-*x*/CC (*x* = 4, 5 and 6) gradually increases from 71.69 to 238.61 μmol·g^{-1} with the increase of the γ-Al_2O_3 content, indicating that abundant NOx species are adsorbed on CS-SiAl-*x*/CC (*x* = 4, 5 and 6). This result is consistent with the In situ DRIFTS observations of NO + O_2 adsorption. Therefore, the plentiful NOx species formed on the CS-SiAl-4/CC are one of the main factors affecting the NOx-SCR performance.

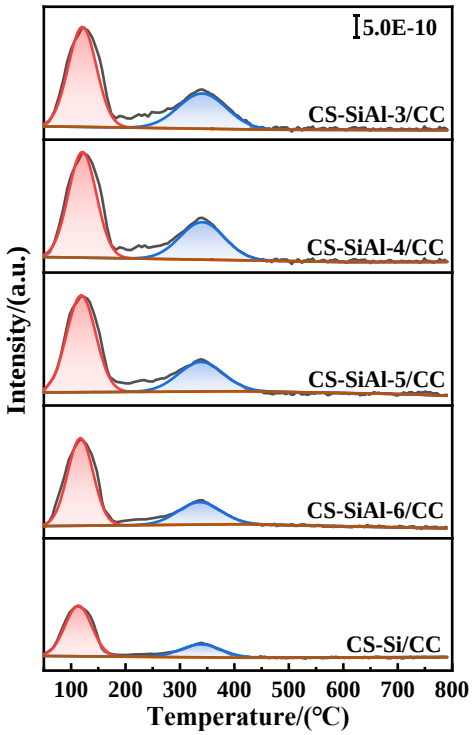

Fig. 7. ($NO+O_2$)-TPD patterns of CS-Si/CC and CS-SiAl-*x*/CC.

Table 3 Changes in NOx storage capacity and acid capacity on CS, CS-Si/CC and CS-SiAl-*x*/CC.

catalysts	[a]($NO+O_2$)-TPD (μmol·g^{-1})			[b]NH_3-TPD (mmol·g^{-1})			
	50–200 ℃	225–445 ℃	Total	Weak acid sites (WACs)	Moderate acid sites (MACs)	Strong acid sites (SACs)	Total
CS	72.20	31.25	103.45	1.69	0.43	0.13	2.25
CS-Si/CC	51.63	20.06	71.69	1.13	0.31	0.11	1.55
CS-SiAl-6/CC	117.10	53.18	170.28	1.24	0.33	0.09	1.66
CS-SiAl-5/CC	136.79	67.78	204.57	1.31	0.35	0.10	1.76
CS-SiAl-4/CC	150.35	88.26	238.61	1.40	0.37	0.10	1.87
CS-SiAl-3/CC	141.27	72.86	214.13	1.23	0.29	0.06	1.58

[a] Analyzed by ($NO+O_2$)-TPD. [b] Analyzed by NH_3-TPD.

3.5 Acid sites

3.5.1 NH_3 adsorption

The acid centers of molecular sieves play a crucial role in activating and reserving NH_3, which is one of the most critical steps in the NH_3-SCR of NOx reaction. The catalysts were pretreated in an Ar atmosphere for 1 h at 400 ℃, followed by purging with Ar for 1 h at 50 ℃. Subsequently, 1000 ppm NH_3 was introduced and its adsorption on CS, CS-Si/CC and CS-SiAl-*x*/CC was collected using in situ

DRIFTS at 50 ℃. As exhibited in Fig. 8, the peaks at around 1457 and 3268 cm^{-1} are attributed to the NH_4^+ ions adsorbed on the Brønsted acid sites [61], while the peaks at around 1605 and 3162 cm^{-1} correspond to the coordinated NH_3 bonded to the Lewis acid sites provided by Cu sites and NH_3 adsorbed on the Lewis acid sites, respectively [62,63]. The peak at around 3339 cm^{-1} is assigned to NH_4^+ ions adsorbed on Si-OH sites [30,63]. Furthermore, the peaks at around 3604, 3681 and 3739 cm^{-1} are ascribed to the NH_3 adsorbed on the Cu-OH, Al-OH and Si-OH sites, respectively [30,61,64]. No change is observed in the NH_3 adsorption species on the SiO_2 and/or γ-Al_2O_3-modified catalysts (Fig. 8a). This result demonstrates that the incorporation of SiO_2 and/or γ-Al_2O_3 does not alter the NH_3 adsorbed species on CS. To investigate the dynamic evolution of adsorbed NH_3 species on CS, CS-Si/CC and CS-SiAl-4/CC, in situ DRIFTS was systematically employed for monitoring, as shown in Fig. 8b-d. For CS, CS-Si/CC and CS-SiAl-4/CC, the peak intensities associated with NH_3 adsorbed species exhibit a gradual enhancement with increasing adsorption time (Fig. 8b-d). Compared with CS, the introduction of SiO_2 leads to an enhancement in peak intensities at around 1456, 1603 and 3739 cm^{-1} accompanied by a reduction in peak intensities at around 3200, 3266 and 3337 cm^{-1}, indicating that SiO_2 may alter the surface acid properties of CS and modulate NH_3 adsorption sites. However, the adsorption strength of NH_4^+ ions on Brønsted acid sites (1454 cm^{-1}) for the CS-SiAl-4/CC is significantly lower than that of the CS and CS-Si/CC. Gao et al [65] proposed that a reduction in Brønsted acid sites leads to significant improvement in catalyst performance. Therefore, it can be inferred that the appropriate γ-Al_2O_3 doping optimizes the surface acidity of CS-SiAl-4/CC, thereby enhancing its catalytic performance.

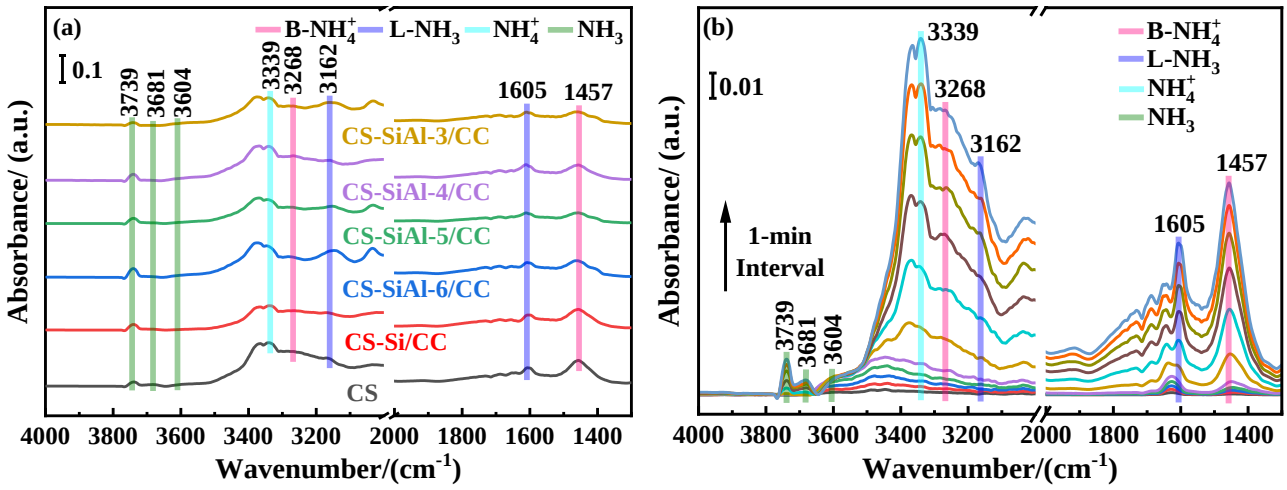

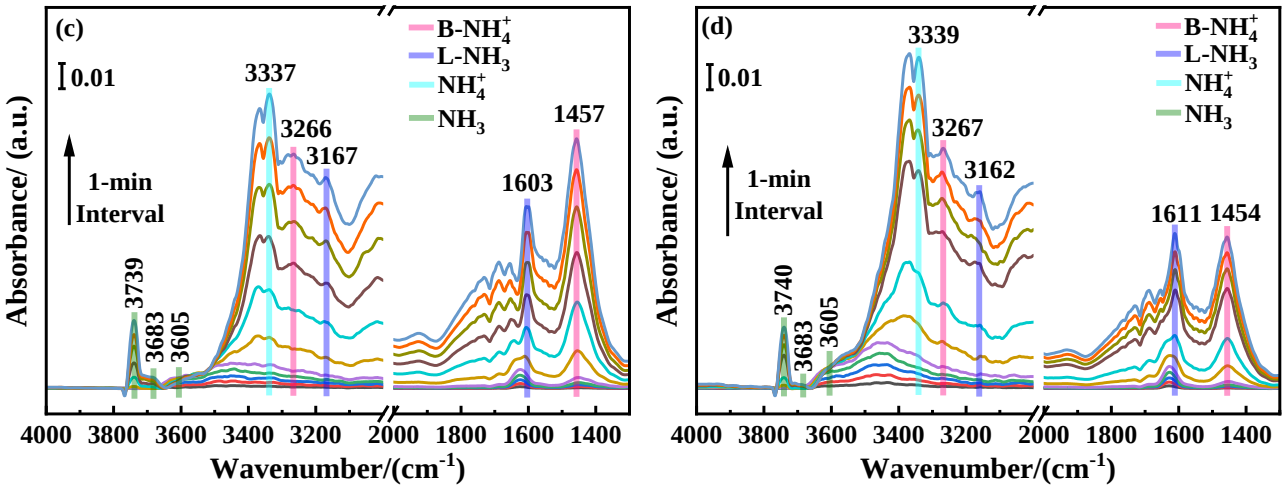

Fig. 8. In situ DRIFTS of NH_3 adsorption on: (a) CS, CS-Si/CC and CS-SiAl-*x*/CC at 50 ℃ at 10 min; (b)–(d) Time-dependent profiles for (b) CS, (c) CS-Si/CC and (d) CS-SiAl-4/CC with exposure durations spanning 1–10 min (at 1 min intervals) at 50 ℃.

3.5.2. NH_3 desorption

The desorption behavior of NH_3 on the catalyst's acid centers was further investigated by NH_3-TPD, and the experimental results are displayed in Fig. 9 and Fig. S6. It can be clearly observed from Fig. 9 that three distinct desorption peaks are observed at around 179, 329 and 436 ℃ for CS-Si/CC and CS-SiAl-*x*/CC, which are attributed to weak acid sites (WACs), medium acid sites (MACs) and strong acid sites (SACs), respectively [41,43,66]. A very interesting phenomenon found in Fig. S6 is that SACs are only dedicated by CS, while WACs and MACs can be contributed to γ-Al_2O_3, SiO_2 and CS. In addition, the intensity of the NH_3 desorption peak on γ-Al_2O_3 is significantly stronger than that on SiO_2 (Fig. S6), indicating that the contribution of γ-Al_2O_3 to WACs and MACs is much higher than that of SiO_2. The acid sites (WACs and MACs) on γ-Al_2O_3 comprise both Brønsted acid sites (from surface hydroxyl groups) and Lewis acid sites (from uncoordinated Al^{3+}). Besides, these acid sites play a very important role in storing NH_3 and providing NH_4^+ [30]. More importantly, NH_3 and NH_4^+ can participate in reactions with NOx species [15,67]. Therefore, the performance of the catalyst is improved to some extent. By performing curve-fitting analysis on the NH_3-TPD spectra, the NH_3 desorption capacities associated with different types of acid sites were quantified and compiled in Table 3. The amount of acid centers on CS-SiAl-*x*/CC (*x* = 4, 5 and 6) gradually enhances from 1.55 to 1.87 mmol·g^{-1} with the increase of γ-Al_2O_3 content. In particular, the amount of the WACs and MACs on CS-SiAl-*x*/CC (*x* = 4, 5 and 6) is always higher than that on the CS-Si/CC. The higher NOx conversion on CS-SiAl-*x*/CC declares that the amount of the WACs and MACs is one of the main

389 factors that can directly affect the NH_3-SCR performance of the catalyst. This finding is consistent
390 with the NH_3-TPD results reported by Wang et al. [30], Liu et al. [35] and Xu et al. [68]. However, the
391 inferior NH_3 adsorption capacity of CS-SiAl-3/CC relative to CS-SiAl-4/CC arises from excessive γ-
392 Al_2O_3 coverage partially obstructing the Cu species. The observed decrease in the catalytic activity of
393 CS-SiAl-3/CC is linked to this phenomenon, as demonstrated by the corresponding NH_3-SCR
394 performance deterioration.

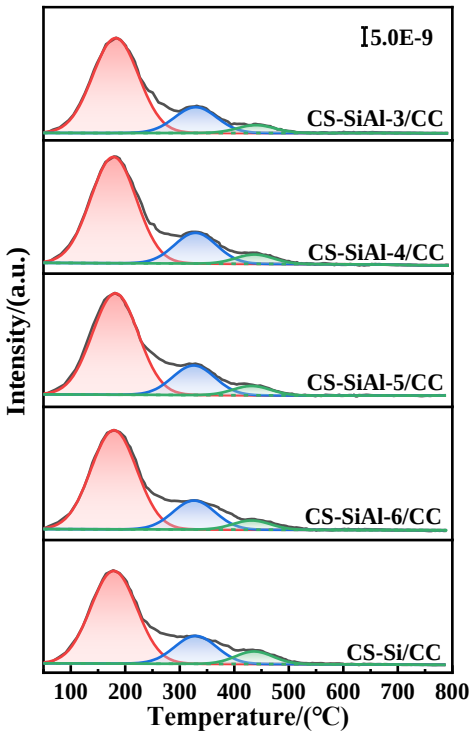

Fig. 9. NH_3-TPD patterns of CS-Si/CC and CS-SiAl-*x*/CC.

395 3.6 Reaction mechanism study

396 3.6.1 Reactions between pre-adsorbed NO + 10% O_2 and NH_3 + 10% O_2

397 Fig. 10 illustrates the dynamic evolution of the reaction between NH_3 + 10% O_2 and pre-adsorbed
398 NO + 10% O_2 at 200 ℃ over time, revealing the NH_3-SCR reaction mechanisms of the CS-Si/CC and
399 CS-SiAl-4/CC. After switching to NH_3 + O_2, the monodentate nitrates (1332 and 1423 cm^{-1}) and free
400 ionic nitrates (1373 cm^{-1}) adsorbed on Cu sites can be rapidly consumed in the SCR reaction. It
401 indicates that both monodentate nitrates and free ionic nitrates play a more critical role as the main
402 active intermediates. Meanwhile, the NH_3 adsorbed on the Lewis acid sites (3162 cm^{-1}) is observed on
403 CS-Si/CC and CS-SiAl-4/CC at 1 min, and its adsorption intensity increases with prolonged reaction
404 time. More importantly, the consumption rates of both monodentate nitrate and free ionic nitrate on

CS-SiAl-4/CC are significantly faster than those on CS-Si/CC, and the adsorption strength of NH_3 on the Lewis acid sites on CS-SiAl-4/CC is dramatically higher than that on CS-Si/CC at some point. Moreover, Lyu et al [55] and Xiong et al [69] proposed that NH_3 adsorbed on the Lewis acid sites can react with free ionic nitrates/monodentate nitrates to form N_2 and H_2O. It can be inferred that γ-Al_2O_3 can provide sufficient NH_3 adsorbed on the Lewis acid sites to participate in SCR reaction between NH_3 adsorbed on the Lewis acid sites and free ionic nitrate/monodentate nitrate. As a result, the consumption rates of monodentate nitrate and free ionic nitrate are faster on CS-SiAl-4/CC than on CS-Si/CC during reaction with NH_3 + O_2. In short, the NH_3 adsorbed on the Lewis acid sites reacts with the adsorbed NOx species (monodentate nitrates and free ionic nitrates) through the Langmuir-Hinshelwood (L-H) mechanism to participate in the SCR reaction.

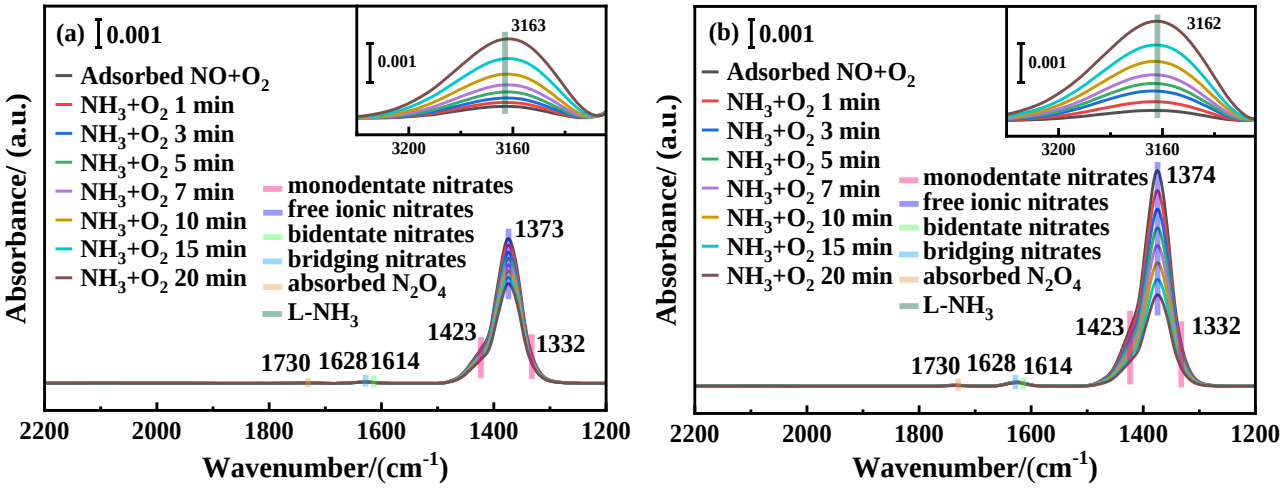

Fig. 10. In situ DRIFTS of pre-adsorbed NO + O_2 followed by reaction with NH_3 + O_2 on (a) CS-Si/CC and (b) CS-SiAl-4/CC at 200 ℃.

3.6.2 Reactions between pre-adsorbed NH_3 + 10% O_2 and NO + 10% O_2

Fig. 11 illustrates the dynamic evolution of the reaction between NO + 10% O_2 and pre-adsorbed NH_3 + 10% O_2 at 200 ℃ over time, revealing the NH_3-SCR reaction mechanisms of the CS-Si/CC and CS-SiAl-4/CC. After switching to NO + O_2, NH_4^+ adsorbed on Brønsted acid sites (1482 and 3266 cm^{-1}) and Si-OH sites (3337 cm^{-1}) is gradually consumed in the SCR reaction, which means that the NH_4^+ plays a more important role as the main active intermediates, and its reaction with gaseous NO indicates the Eley-Rideal (E-R) mechanism. With prolonged exposure of pre-adsorbed NH_3 species to NO + O_2, bidentate nitrates are observed on CS-Si/CC (at 7 min) and CS-SiAl-4/CC (at 5 min). This result indicates that γ-Al_2O_3 can effectively promote the formation of bidentate nitrates. However,

bidentate nitrates can convert to monodentate nitrites to participate in the SCR reaction [35,70], which serve as the active species for the SCR reaction. This might be interpreted as the CS-SiAl-4/CC has superior activity compared to CS-Si/CC. Meanwhile, the NH_3 adsorbed on the Lewis acid sites (3180 cm^{-1}) is consumed rapidly on CS-Si/CC and CS-SiAl-4/CC. It reveals that NH_3 adsorbed on the Lewis acid sites reacts with monodentate nitrites in the SCR reaction through the Langmuir-Hinshelwood (L-H) mechanism.

In the end, based on the above analysis, Fig. 12 depicts the possible synergistic pathways of NH_3-SCR reaction on CS-SiAl-4/CC. γ-Al_2O_3 features a substantial number of both Brønsted and Lewis acid sites, which play a crucial role in storing NH_3 and providing NH_4^+. Furthermore, NH_3 and NH_4^+ serve as the main active intermediates. The reaction consists of NH_3 adsorbed on the Lewis acid sites reacting with free ionic nitrates/monodentate nitrites adsorbed on the Cu sites and gaseous NO reacting with NH_4^+. Therefore, NH_3-SCR reaction on CS-SiAl-4/CC follows L-H and E-R mechanisms.

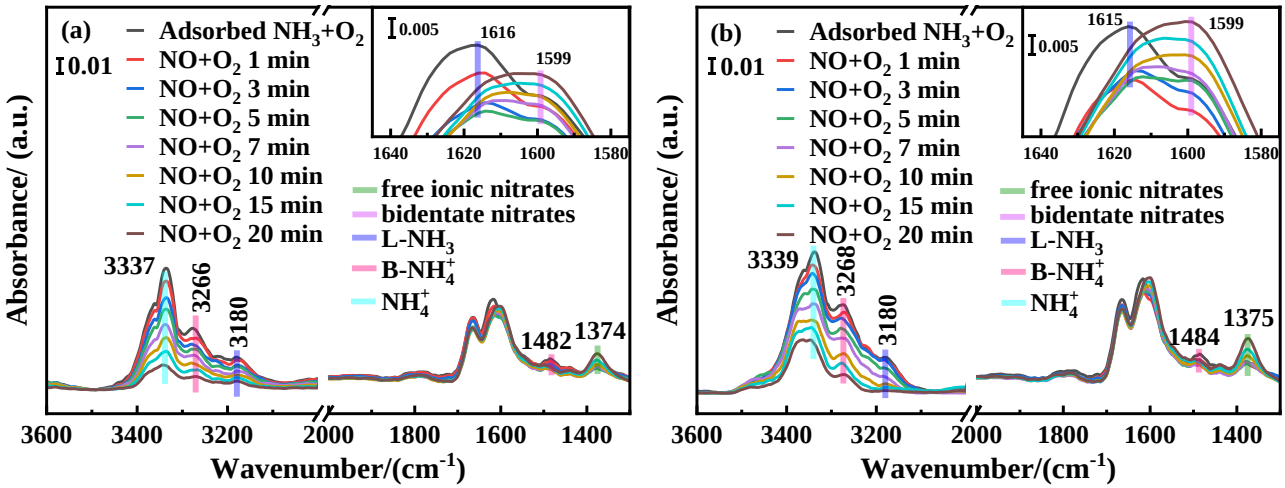

Fig. 11. In situ DRIFTS of pre-adsorbed NH_3 + O_2 followed by reaction with NO + O_2 on (a) CS-Si/CC and (b) CS-SiAl-4/CC at 200 ℃.

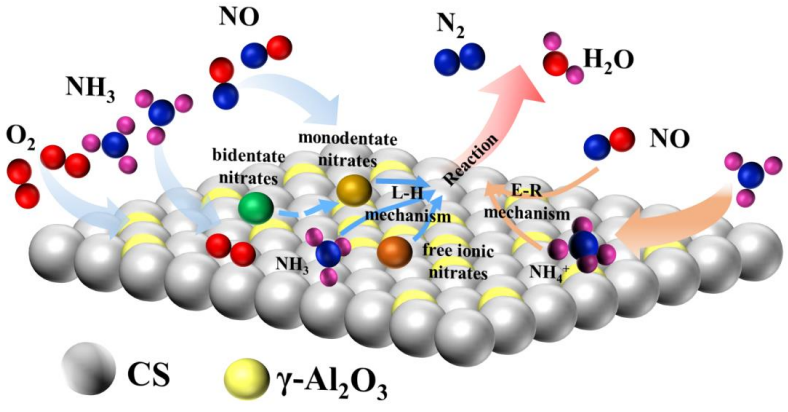

Fig. 12. The possible synergistic pathways of NH_3-SCR reaction on CS-SiAl-4/CC.

4. Conclusion

A series of CS-SiAl-*x*/CC (*x* = 3, 4, 5 and 6) were prepared and evaluated for NH_3-SCR activity. CS-SiAl-4/CC, selected as the optimal catalyst, exhibits remarkable NOx conversion, achieving greater than 80% across a broad temperature range of 218–550 ℃ and over 90% in the narrower window of 245–440 ℃ and displays outstanding N_2 selectivity. Furthermore, this catalyst displays excellent NOx purification performance in the absence of water vapor as well as outstanding hydrothermal aging resistance. γ-Al_2O_3 enhances NOx adsorption capacity and rate, thereby promoting the formation of nitrate intermediate species. Concurrently, γ-Al_2O_3 modulates the relative abundance of NH_4^+ and NH_3, while enhancing the NH_3 adsorption rate on the catalyst. For CS-SiAl-4/CC, the SCR reaction follows both E-R and L-H mechanisms. The reaction consists of gaseous NO reacting with NH_4^+ and NH_3 adsorbed on the Lewis acid sites reacting with free ionic nitrates/monodentate nitrites adsorbed on the Cu sites. More importantly, bidentate nitrates can convert to monodentate nitrites, which serve as the active species for the SCR reaction. This might be interpreted as the CS-SiAl-4/CC having superior activity compared to CS-Si/CC.

CRediT authorship contribution statement

Ruibin Sun: Writing – original draft, Methodology, Investigation, Data curation, Conceptualization. **Yu Lyu:** Investigation, Methodology. **Chonglin Song:** Writing - review & editing, Project administration, Funding acquisition. **Chenxi Wang:** Investigation, Data curation. **Gang Lyu:** Resources, Formal analysis, Conceptualization. **Xiangyu Dong:** Methodology, Investigation, Data curation. **Lei Tian:** Investigation, Data curation. **Xinhui Liu:** Investigation. **Yibo Xu:** Data curation.

Declare of interest statement

The authors declare that they have no known competing financial interests or personal relationships that could have appeared to influence the work reported in this paper.

Acknowledgement

This study was supported by the National Natural Science Foundation of China (Grant number: 51921004, 52176123).

Appendix A. Supplementary data

Supplementary data to this article can be found online at XXX.

Reference

[1] J. J. Corbett, J. J. Winebrake, E. H. Green, P. Kasibhatla, V. Eyring, A. Lauer, Mortality from ship emissions: A global assessment, Environ. Sci. Technol. 41 (2007) 8512–8518, https://doi.org/10.1021/es071686z.

[2] P. C. Guillaume, M. Robert, A. Akshay, C. D. Irene, D. E. Sebastian, L. S. Raymond, R. H. B. Steven, Public health impacts of excess NOx emissions from volkswagen diesel passenger vehicles in Germany, Environ. Res. Lett. 12 (2017) 034014, https://doi.org/10.1088/1748-9326/aa5987.

[3] S. Maciej, J. Nicole, B. Rob, S. Oliver, V. Ilonca, K. Derek, V. D. B. Carolien, L. B. Michiel, D. Martin, B. Bert, H. Gerard, Long-term exposure to particulate matter, NO_2 and the oxidative potential of particulates and diabetes prevalence in a large national health survey, Environ. Int. 108 (2017) 228–236, https://doi.org/10.1016/j.envint.2017.08.017.

[4] Q. Lu, Z. Ali, H. Tang, T. Iqbal, Z. Arain, M. Cui, D. Liu, W. Li, Y. Yang, Regeneration of commercial SCR catalyst deactivated by arsenic poisoning in coal-fired power plants, Korean J. Chem. Eng. 36 (2019) 377–384, https://doi.org/10.1007/s11814-018-0227-9.

[5] K. Boriboonsomsin, T. Durbin, G. Scora, K. Johnson, D. Sandez, A. Vu, Y. Jiang, A. Burnette, S. Yoon, J. Collins, Z. Dai, C. Fulper, S. Kishan, M. Sabisch, D. Jackson, Real-world exhaust temperature profiles of on-road heavy-duty diesel vehicles equipped with selective catalytic reduction, Sci. Total Environ. 634 (2018) 909–921, https://doi.org/10.1016/j.scitotenv.2018.03.362.

[6] Z. Gholami, G. Luo, F. Gholami, F. Yang, Recent advances in selective catalytic reduction of NOx by carbon monoxide for flue gas cleaning process: a review, Catal. Rev. Sci. Eng. 63 (2021) 68–119, https://doi.org/10.1080/01614940.2020.1753972.

[7] J. Li, H. Chang, L. Ma, J. Hao, R. T. Yang, Low-temperature selective catalytic reduction of NOx with NH_3 over metal oxide and zeolite catalysts–A review, Catal. Today 175 (2011) 147–156, https://doi.org/10.1016/j.cattod.2011.03.034.

[8] Y. Huang, Z. Yu, M. Guo, H. Liu, X. Liu, J. Han, S. Cui, B. Liu, Y. Zhao, J. Wei, B. Liu, S. Chen, Coated monolithic catalysts for better selective catalytic reduction: Concerns about structural integrity, catalytic activity and anti-poisoning performance, Catal. Commun. 178 (2023) 106667, https://doi.org/10.1016/j.catcom.2023.106667.

[9] T. Zhou, L. Li, J. Cheng, Z. Hao, Preparation of binary washcoat deposited on cordierite substrate for catalytic applications, Ceram. Int. 36 (2010) 529–534, https://doi.org/10.1016/j.ceramint.2009.09.027.

[10] L. Tang, Z. Zhao, K. Li, X. Yu, Y. Wei, J. Liu, Y. Peng, Y. Li, Y. Chen, Highly active monolith catalysts of $LaKCoO_3$ perovskite-type complex oxide on alumina-washcoated diesel particulate filter and the catalytic performances for the combustion of soot, Catal. Today 339 (2020) 159–173, https://doi.org/10.1016/j.cattod.2019.07.039.

[11] L. Tang, Z. Zhao, Y. Wei, J. Liu, Y. Peng, K. Li, Study on the coating of nano-particle and 3DOM $LaCoO_3$ perovskite-type complex oxide on cordierite monolith and the catalytic performances for soot oxidation: The effect of washcoat materials of alumina, silica and titania, Catal. Today 297 (2017) 131–142, http://dx.doi.org/10.1016/j.cattod.2017.06.016.

[12] P. Kyriienko, N. Popovych, S. Soloviev, S. Orlyk, S. Dzwigaj, Remarkable activity of Ag/Al_2O_3/cordierite catalysts in SCR of NO with ethanol and butanol, Appl. Catal. B: Environ. 140–141 (2013) 691–699, https://doi.org/10.1016/j.apcatb.2013.04.067.

[13] C. Wang, F. Yu, M. Zhu, X. Wang, J. Dan, J. Zhang, P. Cao, B. Dai, Microspherical MnO_2-CeO_2-Al_2O_3 mixed oxide for monolithic honeycomb catalyst and application in selective catalytic reduction of NOx with NH_3 at 50–150°C, Chem. Eng. J. 346 (2018) 182–192, https://doi.org/10.1016/j.cej.2018.04.033.

[14] Y. Qiu, B. Liu, J. Du, Q. Tang, Z. Liu, R. Liu, C. Tao, The monolithic cordierite supported V_2O_5–MoO_3/TiO_2 catalyst for NH_3-SCR, Chem. Eng. J. 294 (2016) 264–272, https://doi.org/10.1016/j.cej.2016.02.094.

[15] S. Xu, J. Li, Q. Lin, H. Xu, J. Wang, Y. Chen, Engineering CeZrOx-Cu/SSZ-13 coupled catalysts to synergistically enhance the low-temperature NH_3-SCR activity, Chem. Eng. J. 476 (2023) 146767, https://doi.org/10.1016/j.cej.2023.146767.

[16] X. Tang, C. Wang, F. Gao, W. Han, H. Yi, S. Zhao, Y. Zhou, Y. Liu, Mn-Fe-Ce multiple oxides with Al_2O_3 coating supported onto honeycomb cordierite monoliths for NO catalytic oxidation, Colloids Surf. A Physicochem. Eng. Asp. 611 (2021) 125790, https://doi.org/10.1016/j.colsurfa.2020.125790.

[17] L. Lisi, R. Pirone, G. Russo, V. Stanzione, Cu-ZSM5 based monolith reactors for NO decomposition, Chem. Eng. J. 154 (2009) 341–347, https://doi.org/10.1016/j.cej.2009.04.025.

[18] J. Shi, Z. Zhang, M. Chen, Z. Zhang, W. Shangguan, S. Gu, H. Shin-ichi, Effect of alumina and zirconia as binders on the activity of Fe-BEA for NH_3-SCR of NO, Front. Environ. Sci. Eng. 12 (2018) 15, https://doi.org/10.1007/s11783-018-1012-4.

[19] R. Zhang, K. Hedjazi, B. Chen, Y. Li, Z. Lei, N. Liu, M(Fe, Co)-BEA washcoated honeycomb cordierite for N_2O direct decomposition, Catal. Today 273 (2016) 273–285, https://doi.org/10.1016/j.cattod.2016.03.021.

[20] F. Wang, J. Ma, S. Xin, Q, Wang, J. Xu, C. Zhang, H. He, X. Zeng, Resolving the puzzle of single-atom silver dispersion on nanosized γ-Al_2O_3 surface for high catalytic performance, Nat. Commun. 11 (2020) 529, https://doi.org/10.1038/s41467-019-13937-1.

[21] L. Sheng, Z. Ma, S. Chen, J. Lou, C. Li, S. Li, Z. Zhang, Y. Wang, H. Yang, Mechanistic insight into N_2O formation during NO reduction by NH_3 over Pd/CeO_2 catalyst in the absence of O_2, Chin. J. Catal. 40 (2019) 1070–1077, https://doi.org/10.1016/S1872-2067(19)63328-0.

[22] T. Liu, S. Su, L. Liu, Q, Yu, K. Xu, L. Jiang, J. Xu, Y. Wang, S. Hu, J. Xiang, Mechanistic investigation of the suppressed N_2O formation during the low-temperature NH_3-SCR over the Sb-modified Mn/Ti catalyst, Chem. Eng. J. 499 (2024) 156301, https://doi.org/10.1016/j.cej.2024.156301.

[23] Y. Zhu, W. Shan, Z. Lian, J. Liu, Y. Zhang, H. He, Effects of impregnation sequence on the NH_3-SCR activity and hydrothermal stability of a Ce-Nb/SnO_2 catalyst, J. Environ. Sci. 138 (2024) 450–457, https://doi.org/10.1016/j.jes.2023.04.032.

[24] X. Yao, L. Chen, T. Kong, S. Ding, Q. Luo, F. Yang, Support effect of the supported ceria-based catalysts during NH_3-SCR reaction, Chin. J. Catal. 38 (2017) 1423–1430, https://doi.org/10.1016/S1872-2067(17)62868-7.

[25] H. Zhou, M. Ge, S. Wu, B. Ye, Y. Su, Iron based monolithic catalysts supported on Al_2O_3, SiO_2, and TiO_2: A comparison for NO reduction with propane, Fuel, 220 (2018) 330–338, https://doi.org/10.1016/j.fuel.2018.01.077.

[26] F. Bin, C. Song, G. Lv, J. Song, S. Wu, X. Li, Selective catalytic reduction of nitric oxide with ammonia over zirconium-doped copper/ZSM-5 catalysts, Appl. Catal. B: Environ. 150–151 (2014) 532–543, http://dx.doi.org/10.1016/j.apcatb.2013.12.052.

[27] L. Xie, F. Liu, L. Ren, X. Shi, F. Xiao, H. He, Excellent performance of one-pot synthesized Cu-SSZ-13 catalyst for the selective catalytic reduction of NOx with NH_3, Environ. Sci. Technol. 48 (2014) 566–572, https://doi.org/10.1021/es4032002.

[28] Y. Shan, W. Shan, X. Shi, J. Du, Y. Yu, H. He, A comparative study of the activity and hydrothermal stability of Al-rich Cu-SSZ-39 and Cu-SSZ-13, Appl. Catal. B: Environ. 264 (2020) 118511, https://doi.org/10.1016/j.apcatb.2019.118511.

[29] X. Wang, Y. Xu, M. Qin, Z. Zhao, X. Fan, Q. Li, Insight into the effects of Cu^{2+} ions and CuO species in Cu-SSZ-13 catalysts for selective catalytic reduction of NO by NH_3, J. Colloid Interface Sci. 622 (2022) 1–10, https://doi.org/10.1016/j.jcis.2022.04.110.

[30] J. Wang, J. Liu, X. Tang, C. Xing, T. Jin, The promotion effect of niobium on the low-temperature activity of Al-rich Cu-SSZ-13 for selective catalytic reduction of NOx with NH_3, Chem. Eng. J. 418 (2021) 129433, https://doi.org/10.1016/j.cej.2021.129433.

[31] Q. Lin, S. Xu, H. Zhao, S. Liu, H. Xu, Y. Dan, Y. Chen, Highlights on key roles of Y on the hydrothermal stability at 900 ℃ of Cu/SSZ-39 for NH_3-SCR, ACS Catal. 12 (2022) 14026–14039, https://doi.org/10.1021/acscatal.2c03757.

[32] S. Mohan, P. Dinesha, S. Kumar, NOx reduction behaviour in copper zeolite catalysts for ammonia SCR systems: A review, Chem. Eng. J. 384 (2020), 123253, https://doi.org/10.1016/j.cej.2019.123253.

[33] M. Chen, Y. Wei, J. Han, W. Yan, J. Yu, Enhancing catalytic performance of Cu-SSZ-13 for the NH_3-SCR reaction via in situ introduction of Fe^{3+} with diatomite, Mater. Chem. Front. 5 (2021), 7787–7795, https://doi.org/10.1039/D1QM01101D.

[34] A. Wang, K. Xie, D. Bernin, A. Kumar, K. Kamasamudram, L. Olsson, Deactivation mechanism of Cu active sites in Cu/SSZ-13 — Phosphorus poisoning and the effect of hydrothermal aging, Appl. Catal. B: Environ. 269 (2020), 118781, https://doi.org/10.1016/j.apcatb.2020.118781.

[35] Q. Liu, Z. Fu, L. Ma, H. Niu, C. Liu, J. Li, Z. Zhang, MnOx-CeO_2 supported on Cu-SSZ-13: A novel SCR catalyst in a wide temperature range, Appl. Catal. A Gen. 547 (2017) 146–154, https://doi.org/10.1016/j.apcata.2017.08.024.

[36] Y. Ma, Z. Li, N. Zhao, Y. Teng, One-pot synthesis of Cu–Ce co-doped SAPO-5/34 hybrid crystal structure catalysts for NH_3-SCR reaction with SO_2 resistance, J. Rare Earths 39 (2021), 1217–1223, https://doi.org/10.1016/j.jre.2020.07.028.

[37] M. Xie, X. Xiao, J. Wang, J. Chen, H. Kang, N. Wang, W. Chu, L. Li, Mechanistic insights into the cobalt promotion on low-temperature NH_3-SCR reactivity of Cu/SSZ-13, Sep. Purif. Technol. 315 (2023) 123617, https://doi.org/10.1016/j.seppur.2023.123617.

583 [38] M. Chen, W. Zhao, Y. Wei, J. Han, J. Li, C. Sun, D. Mei, J. Yu, La ions-enhanced NH_3-SCR
584 performance over Cu-SSZ-13 catalysts, Nano Res. 16 (2023) 12126–12133,
585 https://doi.org/10.1007/s12274-023-5500-x.
586 [39] D. Deng, S. Deng, D. He, Z. Wang, Z. Chen, Y. Ji, G. Yan, G. Hou, L. Liu, H. He, A comparative
587 study of hydrothermal aging effect on cerium and lanthanum doped Cu/SSZ-13 catalysts for NH_3-SCR,
588 J. Rare Earths 39 (2021) 969–978, https://doi.org/10.1016/j.jre.2020.08.016.
589 [40] J. Song, Y. Wang, E. D. Walter, N. M. Washton, D. Mei, L. Kovarik, M. H. Engelhard, S.
590 Prodinger, Y. Wang, C. H. F. Peden, F. Gao, Toward rational design of Cu/SSZ-13 selective catalytic
591 reduction catalysts: Implications from atomic-level understanding of hydrothermal stability, ACS
592 Catal. 7 (2017) 8214–8227, https://doi.org/10.1021/acscatal.7b03020.
593 [41] C. Fan, Z. Chen, L. Pang, S. Ming, C. Dong, K. Brou Albert, P. Liu, J. Wang, D. Zhu, H. Chen,
594 T. Li, Steam and alkali resistant Cu-SSZ-13 catalyst for the selective catalytic reduction of NOx in
595 diesel exhaust, Chem. Eng. J. 334 (2018) 344–354, https://doi.org/10.1016/j.cej.2017.09.181.
596 [42] J. Liu, X. Tang, C. Xing, T. Jin, Y. Yin, J. Wang, Niobium modification for improving the high-
597 temperature performance of Cu-SSZ-13 in selective catalytic reduction of NO by NH_3, J. Solid State
598 Chem. 296 (2021) 122028.
599 [43] R. Xu, Z. Wang, N. Liu, C. Dai, J. Zhang, B. Chen, Understanding Zn functions on hydrothermal
600 stability in a one-pot-synthesized Cu&Zn-SSZ-13 catalyst for NH_3 selective catalytic reduction, ACS
601 Catal. 10 (2020) 6197–6212.
602 [44] M. Chen, J. Li, W. Xue, S. Wang, J. Han, Y. Wei, D. Mei, Y. Li, J. Yu, Unveiling secondary-ion-
603 promoted catalytic properties of Cu/SSZ-13 zeolites for selective catalytic reduction of NOx. J. Am.
604 Chem. Soc. 144 (2022) 12816–12824. https://doi.org/10.1021/jacs.2c03877.
605 [45] C. Niu, X. Shi, F. Liu, K. Liu, L. Xie, Y. You, H. He, High hydrothermal stability of Cu–SAPO-
606 34 catalysts for the NH3-SCR of NOx, Chem. Eng. J. 294 (2016) 254–263,
607 https://doi.org/10.1016/j.cej.2016.02.086.
608 [46] N. Reddy, P. Bera, V. Reddy, N. Sridhara, A. Dey, C. Anandan, A. Sharma, XPS study of
609 sputtered alumina thin films, Ceram. Int. 40 (2014) 11099–11107,
610 https://doi.org/10.1016/j.ceramint.2014.03.133.
611 [47] Y. He, L. Zhang, X. An, G. Wan, W. Zhu, Y. Luo, Enhanced fluoride removal from water by rare
612 earth (La and Ce) modified alumina: Adsorption isotherms, kinetics, thermodynamics and mechanism,

Sci. Total Environ. 688 (2019) 184–198, https://doi.org/10.1016/j.scitotenv.2019.06.175.

[48] H. Wang, R. Xu, Y. Jin, R. Zhang, Zeolite structure effects on Cu active center, SCR performance and stability of Cu-zeolite catalysts, Catal. Today 327 (2019) 295–307, https://doi.org/10.1016/j.cattod.2018.04.035

[49] A. K. S. Clemens, A. Shishkin, P. A. Carlsson, M. Skoglundh, F. J. Martínez-Casado, Z.MatěJ, O. Balmes, H. Harelind, Reaction-driven ion exchange of copper into zeolite SSZ-13, ACS Catal. 5 (2015) 6209–6218, https://doi.org/10.1021/acscatal.5b01200.

[50] Z. Zhao, R. Yu, R. Zhao, C. Shi, H. Gies, F. Xiao, D. D. Vos, T. Yokoi, X. Bao, U. Kolb, M. Feyen, R. McGuire, S. Maurer, A. Moini, U. Müller, W. Zhang, Cu-exchanged Al-rich SSZ-13 zeolite from organotemplate-free synthesis as NH_3-SCR catalyst: Effects of Na^+ ions on the activity and hydrothermal stability, Appl. Catal. B: Environ. 217 (2017) 421–428, https://doi.org/10.1016/j.apcatb.2017.06.013.

[51] K. Leistner, A. Kumar, K. Kamasamudram, L. Olsson, Mechanistic study of hydrothermally aged Cu/SSZ-13 catalysts for ammonia-SCR, Catal. Today 307 (2018) 55–64. https://doi.org/10.1016/j.cattod.2017.04.015.

[52] D. L. Wu, V. Tschamber, L. Limousy, J. Klein, A. Westermann, B. Azambre, I. Fechete, F. Garin, Simultaneous effect of carbon and water on NOx adsorption on a stabilized Pt-Ba/Al_2O_3 catalyst, C. R. Chim. 17 (2014) 687–700.

[53] J. J. Yu, Z. Jiang, L. Zhu, Z. P. Hao, Z. P. Xu, Adsorption/Desorption studies of NOx on well-mixed oxides derived from Co-Mg/Al hydrotalcite-like compounds, J. Phys. Chem. B 110 (2006) 4291–4300, https://doi.org/10.1021/jp056473f.

[54] W. Su, H. Chang, Y. Peng, C. Zhang, J. Li, Reaction pathway investigation on the selective catalytic reduction of NO with NH_3 over Cu/SSZ-13 at low temperatures, Environ. Sci. Technol. 49 (2015) 467–473, https://doi.org/10.1021/es503430w.

[55] Y. Lyu, G. Lyu, R. Sun, C. Song, Insights into copper-ZSM-5 supported cerium, zirconium catalysts to promote NH_3-SCR activity and anti-thermal aging performance, Fuel 367 (2024) 131456, https://doi.org/10.1016/j.fuel.2024.131456.

[56] B. Li, C. Song, G. Lv, K. Chen, X. Cao, Impact of soot on NOx adsorption over Cu-modified hydrotalcite-derived lean NOx trap catalyst, Langmuir 33 (2017) 2939–2948, https://doi.org/10.1021/acs.langmuir.6b03877.

643 [57] H. Kubota, C. Liu, T. Toyao, Z. Maeno, M. Ogura, N. Nakazawa, S. Inagaki, Y. Kubota, K.
644 Shimizu, Formation and reactions of NH_4NO_3 during transient and steady-state NH_3-SCR of NOx over
645 H-AFX zeolites: Spectroscopic and theoretical studies, ACS Catal. 10 (2020) 2334–2344,
646 https://doi.org/10.1021/acscatal.9b05151.
647 [58] Y. Wang, G. Li, S. Zhang, X. Zhang, X, Zhang, Z. Hao, Promoting effect of Ce and Mn addition
648 on Cu-SSZ-39 zeolites for NH_3-SCR reaction: Activity, hydrothermal stability, and mechanism study,
649 Chem. Eng. J. 393 (2020) 124782, https://doi.org/10.1016/j.cej.2020.124782.
650 [59] X. Wang, T. Li, C. Wang, Q. Cui, T. Wang, X. Bao, Y. Yue, Improving catalytic performance of
651 Cu-SSZ-13 for NOx abatement via in-situ introduction of La and Ce from spent catalyst, Sep. Purif.
652 Technol. 331 (2024) 125638, https://doi.org/10.1016/j.seppur.2023.125638.
653 [60] H. Jiang, B. Guan, X. Peng, R. Zhan, H. Lin, Z. Huang, Influence of synthesis method on catalytic
654 properties and hydrothermal stability of Cu/SSZ-13 for NH_3-SCR reaction, Chem. Eng. J. 379 (2020)
655 122358, https://doi.org/10.1016/j.cej.2019.122358.
656 [61] F. Gao, N. M. Washton, Y. Wang, M. Kollár, J. Szanyi, C. H. F. Peden, Effects of Si/Al ratio on
657 Cu/SSZ-13 NH_3-SCR catalysts: Implications for the active Cu species and the roles of Brønsted acidity,
658 J. Catal. 331 (2015) 25–38, https://doi.org/10.1016/j.jcat.2015.08.004.
659 [62] S. Han, J. Cheng, C. Zheng, Q. Ye, S. Cheng, T. Kang, H. Dai, Effect of Si/Al ratio on catalytic
660 performance of hydrothermally aged Cu-SSZ-13 for the NH_3-SCR of NO in simulated diesel exhaust,
661 Appl. Surf. Sci. 419 (2017) 382–392, https://doi.org/10.1016/j.apsusc.2017.04.198.
662 [63] J. Luo, D. Wang, A. Kumar, J. Li, K. Kamasamudram, N. Currier, A. Yezerets, Identification of
663 two types of Cu sites in Cu/SSZ-13 and their unique responses to hydrothermal aging and sulfur
664 poisoning, Catal. Today 267 (2016) 3–9, https://doi.org/10.1016/j.cattod.2015.12.002.
665 [64] D. Wang, Y. Jangjou, Y. Liu, M. K. Sharma, J. Luo, J. Li, K. Kamasamudram, W. S. Epling, A
666 comparison of hydrothermal aging effects on NH_3-SCR of NOx over Cu-SSZ-13 and Cu-SAPO-34
667 catalysts, Appl. Catal. B: Environ. 165 (2015) 438–445, https://doi.org/10.1016/j.apcatb.2014.10.020.
668 [65] F. Gao, Y. Wang, N. M. Washton, M. Kollár, J. Szanyi, C. H. F. Peden, Effects of alkali and
669 alkaline earth cocations on the activity and hydrothermal stability of Cu/SSZ-13 NH_3-SCR catalysts,
670 ACS Catal. 5 (2015) 6780–6791, https://doi.org/10.1021/acscatal.5b01621.
671 [66] Z. Chen, C. Bian, C. Fan, T. Li, The role of Si coordination structures in the catalytic properties
672 and durability of Cu-SAPO-34 as NH_3-SCR catalyst for NOx reduction, Chin. Chem. Lett. 33 (2022)

893–897, https://doi.org/10.1016/j.cclet.2021.06.071.

[67] J. Liang, Y. Mi, G. Song, H. Peng, Y. Li, R. Yan, W. Liu, Z. Wang, P. Wu, F. Liu, Environmental benign synthesis of nano-SSZ-13 via FAU transcrystallization: Enhanced NH_3-SCR performance on Cu-SSZ-13 with nano-size effect, J. Hazard. Mater. 398 (2020) 122986, https://doi.org/10.1016/j.jhazmat.2020.122986.

[68] M. Xu, J. Wang, T. Yu, J. Wang, M. Shen, New insight into Cu/SAPO-34 preparation procedure: Impact of NH_4-SAPO-34 on the structure and Cu distribution in Cu-SAPO-34 NH_3-SCR catalysts, Appl. Catal. B: Environ. 220 (2018) 161–170, https://doi.org/10.1016/j.apcatb.2017.08.031.

[69] S. Xiong, Y. Liao, X. Xiao, H. Dang, S. Yang, the mechanism of the effect of H_2O on the low temperature selective catalytic reduction of NO with NH_3 over Mn-Fe spinel, Catal. Sci. Technol. 5 (2015) 2132–2140, https://doi.org/10.1039/C4CY01599A.

[70] S. Zhan, M. Qiu, S. Yang, D. Zhu, H. Yu, Y. Li, Facile preparation of MnO_2 doped Fe_2O_3 hollow nanofibers for low temperature SCR of NO with NH_3, J. Mater. Chem. A 2 (2014) 20486–20493, https://doi.org/10.1039/C4TA04807E.